Journal Name

ARTICLE TYPE

Cite this: DOI: 00.0000/xxxxxxxxxx

Dynamics of droplets on cones: Self-propulsion due to curvature gradients

John McCarthy,[a] Dominic Vella,[b] and Alfonso A. Castrejón-Pita[a]

Received Date
Accepted Date

DOI: 00.0000/xxxxxxxxxx

We study the dynamics of droplets driven by a gradient of curvature, as may be achieved by placing a drop on the surface of a cone. The curvature gradient induces a pressure gradient within the drop, which in turn leads to spontaneous propulsion of the droplet. To investigate the resulting driving force we perform a series of experiments in which we track a droplet's displacement, s, from the apex of a cone whose surface is treated to exhibit near-zero pinning effects. We find an $s \sim t^{1/4}$ scaling at sufficiently late times t. To shed light upon these dynamics, we perform an asymptotic calculation of the equilibrium shape of a droplet on a weakly curved cylinder, deriving the curvature-induced force responsible for its propulsion. By balancing this driving force with viscous dissipation, we recover a differential equation for the droplet displacement, whose predictions are found to be in good agreement with our experimental results.

1 Introduction

Controlled droplet motion is an area of microfluidics that has received much attention in recent decades. This interest is due to the ubiquity of droplet motion in technological developments such as diagnostics[1], fog harvesting[2,3] and cooling.[4] When there is an imbalance in the forces acting on a droplet, spontaneous motion can occur. Such imbalances can be achieved either by introducing gradients in the surface tension forces acting on the droplet or by the effect of geometry. Gradients in surface tension can be induced by exploiting the dependency of surface energy on surface chemistry[5] or substrate temperature.[6] Geometric gradients can be introduced by placing drops in wedges[7–9], on wedge-like substrates[10] or indeed, on and inside conical substrates.[11–13]

This paper is concerned with spontaneous droplet motion on conical substrates, which is induced by the change in curvature along the axis of the cone. This 'curvotaxis'[13] has been observed extensively in nature, being suggested as an important mechanism in dew drops forming on spider webs[14], cacti remaining hydrated in arid environments[15] and the repulsion of water from within the hairy texturing of the legs of the common water strider.[16] Similarly, curvotaxis has found applications in industry, being proposed as a mechanism to remove micron sized droplets of oil from water using arrays of cones[17] while surfaces decorated with conical microposts have shown promise as a means of producing anti-fogging water repellent surfaces.[18] Despite these promising technologies, only recently have studies described the origin of the force driving droplet motion in detail.[13,19,20]

Drops on cylindrical and conical fibres can adopt two different morphologies, "barrel" and "clamshell" (see Fig. 1). A drop in a barrel configuration completely engulfs a portion of the fibre (and hence is symmetric about the axis of the cone, with two circular contact lines). In contrast, a drop in the clamshell state sits on part of the fibre, without engulfing it, and, as a result, has a single contact line (which is not circular). Which of these shapes a particular drop adopts depends on its volume, the radius of the fibre and its wettability. In general, drops that are large relative to the fibre radius tend to adopt the barrel configuration as do droplets with smaller contact angles.[21–23] The behaviour of droplets can be quite different depending on which morphology is exhibited. In particular, barrel-shaped droplets on conical fibres have a well-defined equilibrium position[24] (even for perfectly wetting liquids), while clamshell droplets on cones do not have such an equilibrium in the absence of external forces such as gravity.[13,19,20] Clamshell droplets therefore move indefinitely along the cone towards the region of lower curvature (independently of wettability) while barrel-shaped droplets simply move to their equilibrium position.[25]

Clamshell droplets have received considerably less attention than barrel-shaped droplets despite being central to many technological applications of droplet motion.[17,26,27] Simulations have been able to provide some qualitative descriptions of clamshell droplets such as the equilibrium position in the presence of gravity[28]; such simulations have also shown that the free energy of the droplet decreases with curvature.[24] As a result, clamshell droplets on the outside of a cone always move to the wider end of the cone independent of wettability.[13] Lv *et al.*[13] presented simu-

[a] *Department of Engineering Science, University of Oxford, Parks Road, Oxford OX1 3PJ, UK. Tel: +44 (0)1865 277921;E-mail: alfonso.castrejon-pita@eng.ox.ac.uk*
[b] *Mathematical Institute, University of Oxford, Woodstock Road, Oxford, OX2 6GG,UK.*

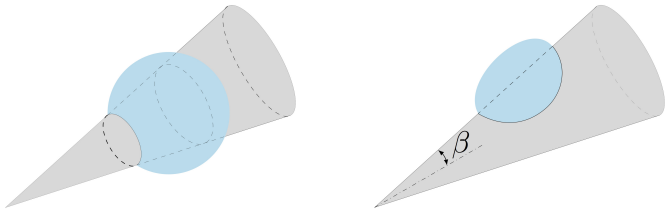

Fig. 1 The two morphologies a droplet may adopt on conical or cylindrical fibres: (a) an axisymmetric barrel engulfing the cone and (b) a clamshell that sits on the side of the cone. Which configuration the droplet adopts depends on its volume, the fibre radius and contact angle. Here, we focus on the case of clamshell droplets.

lations, theoretical calculations and experimental evidence to describe the dynamics of clamshell droplets on cones. They studied the motion of small droplets of water on pulled-glass capillaries which had a significant variation of cone angle along their length (and hence a non-constant curvature gradient). While bulk motion of the droplet was observed, spreading was also a prominent feature, obfuscating the role played by curvature gradients. Moreover, the underlying reason for *why* droplets move towards the region of lower curvature, independent of wettability, remains unclear. The calculations presented by Lv *et al.* [13] considered drops in equilibrium on *spherical* substrates. While this approach provided good agreement between the model, simulations, and experiments, details of the droplet shape on a conical substrate and how the contact line changes remained unclear. Galatola [19] used a more detailed theoretical study of the conical geometry and found good agreement between his model and the experimental results of Lv *et al.* [13], albeit with the aid of a fitting parameter ζ that represents the contact line viscosity. This contact line viscosity is assumed to be the only mechanism of viscous dissipation but was fitted separately for each experiment.

In this work we will study the dynamics of clamshell droplets on conical substrates where spreading and contact line pinning are minimized. To achieve this, we use slippery liquid-infused porous surfaces or "SLIPS".[29] These are surfaces which are coated in a lubricating layer of oil retained by a microscructure on the surface. Such surfaces reduce contact line pinning allowing droplets to move with ease. A wetting-ridge of oil where the contact line would otherwise be is then responsible for viscous dissipation. We make use of previous experimental results that have quantified the viscous dissipation for droplets on a SLIPS in model settings.[30,31] We will also consider the equilibrium shape of a droplet on a cylindrical substrate to understand the contact line behaviour and gain some understanding of why the direction of droplet motion is independent of wettability.

The outline of this paper is as follows: In the next section, we describe the experimental procedure and present preliminary findings. We present a mathematical model of the problem in Section 3 and show that it accounts for our observations. Lastly, in Section 4 we discuss non-conical substrates.

2 Experimental results

Conical Slippery-Liquid-Infused Porous Substrates (SLIPS) were constructed by first manufacturing highly polished cones out of brass (see Appendix A) typically a few centimetres in length. The cone half-angle, β, (see Fig. 1) ranged from 5° to 45°. A commercially available aerosol spray (Glaco Mirror Coat Zero) was used to create a microstructure of silica nanoparticles on the surface of the brass. We followed the procedure for the fabrication of SLIPS as described in Guan *et al.* [32] and Keiser *et al.* [30]. Three applications of Glaco were carried out letting the deposited material dry for thirty minutes between each coat. To achieve both wetting and non-wetting conditions with water droplets, two different lubricating oils were used: silicone oil (non-wetting water droplets) and decanol (wetting water droplets).[33] Silicone oils of varying viscosities ranging from 20 cSt to 500 cSt were used to systematically study the effect of the viscosity of the lubricating layer. The apparent contact angles of water droplets on such surfaces have been reported previously with values of $\approx 45°$ and $\approx 105°$ for decanol and silicone oil, respectively[33,34]. Excess lubricant was removed with the aid of compressed air.

Droplets of deionised water of different volumes (0.5, 2, 4 μL) were then deposited onto the cones with a micropipette (Brand Transferpette® S) and the ensuing motion was recorded at 5 frames per second for slow moving droplets and 30 frames per second for faster droplets. Droplet volumes are chosen to be both large enough to be deposited using a micropipette but small enough that the resulting droplet shapes are not significantly influenced by gravity. A representative series of images, Fig. 2, demonstrates that both wetting and non-wetting droplets move towards the base of the cone. Moreover, the motion occurs perpendicular to the direction of gravity and is therefore not driven by the weight of the droplets. Image analysis was carried out using an in-house Matlab code developed to track the position of the droplet's centre, s, measured from the apex of the cone, in each frame. Plotting s as a function of time, t, (Fig. 3) shows that droplets tend to slow down as they move further from the apex; in particular, for sufficiently late times, it appears that $s \sim t^{1/4}$.

3 Mathematical model

To understand the evolution of $s(t)$ shown in the previous section, it is natural to balance the two forces acting on the droplet: the driving force (due to the curvature gradient of the substrate) and the viscous dissipation. To first calculate the curvature-induced force, our general strategy is to consider a small droplet (so that gravity may be neglected) placed on a weakly curved cylinder (a circular cylinder whose radius is large compared to that of the droplet). The curvature of the cylinder deforms the interface of the drop, which in turn changes its surface energy. For weak cylinder curvatures, we anticipate that the change in droplet shape from the spherical cap it adopts on a planar substrate will be small. This facilitates the calculation of the droplet shape and hence its surface energy, which could then be calculated as a function of cylinder radius. Finally, the force acting on the drop may be found as the gradient of this energy (assuming that drop shape perturbations due to the substrate curvature gradient are negligi-

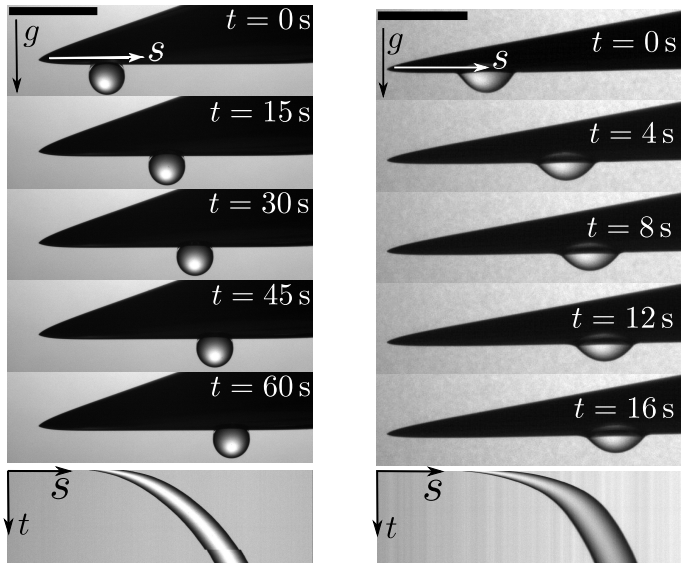

(a) 4μL non-wetting water droplet on a 50 cSt silicone oil SLIP with cone half-angle $\beta = 10^\circ$.

(b) 4μL wetting water droplet on a decanol SLIP with cone half-angle $\beta = 5^\circ$ and $\nu_o = 12$ cSt

Fig. 2 Typical experimental images showing the spontaneous motion of water droplets moving on the outside of conical surfaces. In both non-wetting and wetting states, the droplet moves to the base of the cone so that the distance of the droplet's centre from the cone apex, s, increases. As motion proceeds, droplets tend to slow down, $\mathrm{d}s/\mathrm{d}t \to 0$. This is highlighted in the bottom panes of (a) and (b) which show spatio-temporal plots of drop position created by reslicing the corresponding experimental movie. Note that in each case, the droplet motion occurs perpendicular to the direction in which gravity acts (which is indicated by the white arrow). Scale bars correspond to 5 mm.

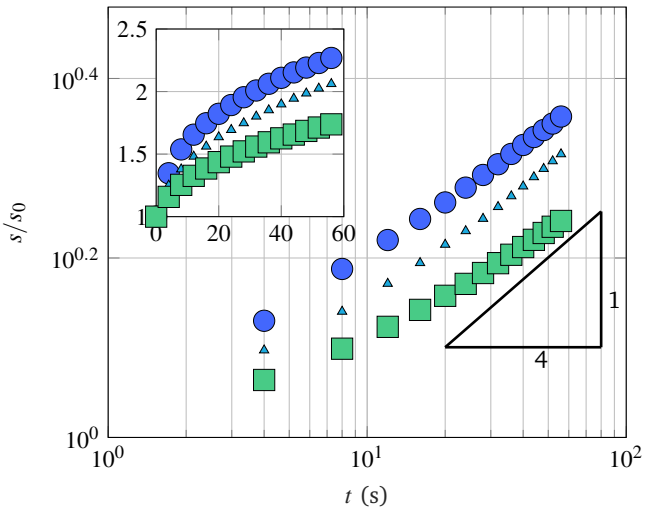

Fig. 3 Main figure: The normalized displacement of the droplet's centre from the cone apex, s/s_0, as a function of time, t, after deposition of the droplet, plotted on logarithmic axes. Marker size denotes droplet volume $V = 4\,\mu$L or $V = 0.5\,\mu$L. The cone half-angle, β, is denoted by marker shape as follows: ●($\beta = 5^\circ$), ▲($\beta = 10^\circ$) and ■($\beta = 20^\circ$). Oil viscosity, ν_o is denoted by colour (blue = 20 cSt, cyan = 50 cSt, green = 500 cSt). All data suggest the scaling $s \sim t^{1/4}$ for late times. Inset: The same data plotted on linear axes.

ble compared to those due to the substrate curvature itself, similar to the assumption of Lorenceau and Quéré [11]; we revisit the assumption following our analysis.

3.1 Capillary driving force

We begin by considering a droplet on a flat substrate, which is known to be a spherical cap; we take the radius of curvature of this droplet to be R_d so that the location of the interface may be written in spherical polar coordinates as $\rho_\mathrm{i} = R_\mathrm{d}$. The substrate is then perturbed to introduce a curvature $1/R_\mathrm{c}$ along one axis as shown in Fig. 4. We let $\varepsilon = R_\mathrm{d}/R_\mathrm{c}$ and assume $\varepsilon \ll 1$. The resulting perturbations are assumed to be regular so that we can pose the expansions:

$$\rho_\mathrm{i}(\phi,\theta) = R_\mathrm{d} + \varepsilon\rho_{\mathrm{i},1}(\phi,\theta) + O(\varepsilon^2), \tag{1}$$

$$\rho_\mathrm{c}(\phi,\theta) = \rho_{\mathrm{c},0}(\phi) + \varepsilon\rho_{\mathrm{c},1}(\phi,\theta) + O(\varepsilon^2), \tag{2}$$

$$p = p_0 + \varepsilon p_1 + O(\varepsilon^2), \tag{3}$$

where, ϕ is the polar angle, θ is the azimuthal angle, see Fig 4 — the specific forms of $\rho_{\mathrm{c},0}, \rho_{\mathrm{c},1}$ and p_0 are given in Appendix B.

The energy of the drop depends on its shape, which is found by solving the Young–Laplace equation coupled with conservation of volume for $\rho_{\mathrm{i},1}(\phi,\theta)$ and p_1. Two boundary conditions at the three-phase contact line (TPCL) must also be satisfied: (1) that the interface must contact the substrate at the TPCL and, (2) that it must do so at a specific contact angle, which we denote by α. More explicitly, we solve the following:

$$p_0 + \varepsilon p_1 = \gamma_\mathrm{lv}\nabla\cdot\boldsymbol{n}_i, \tag{4}$$

$$\rho_\mathrm{i}(\phi,\theta)|_\mathrm{TPCL} = \rho_\mathrm{c}(\phi,\theta), \tag{5}$$

$$\boldsymbol{n}_s\cdot\boldsymbol{n}_i|_\mathrm{TPCL} = \cos\alpha, \tag{6}$$

where the TPCL is parametrised as: $\rho = \rho_\mathrm{c}$ and $\phi = \alpha + \varepsilon f(\theta)$ and symmetry demands that $f(\theta) = a_0 + a_1\cos(2\theta)$.

As expected, a spherical cap $\rho_\mathrm{i} = R_\mathrm{d}$ solves Equations (4)-(6) at leading order. At the next order, the Young–Laplace equation reduces to a Helmholtz type equation (equivalent to Equation (27) of Galatola [19]) which can be solved via separation of variables. Conservation of volume is then imposed to determine the pressure perturbation p_1. Lastly to compute the free energy of the droplet, the liquid–substrate area (A_ls) and the liquid–vapour area (A_lv) can be calculated up to $O(\varepsilon)$ giving,

$$\mathscr{U} = R_\mathrm{d}^2\gamma_\mathrm{lv}\pi(2+\cos\alpha)(1-\cos\alpha)^2 + \varepsilon\gamma_\mathrm{lv}\pi R_\mathrm{d}^2\frac{\sin^4\alpha}{4}, \tag{7}$$

where we have used the fact that $\mathscr{U} = \gamma_\mathrm{lv}(A_\mathrm{lv} - A_\mathrm{ls}\cos\alpha)$.

If we let s denote the distance from the apex of the cone, then the local cylinder radius $R_\mathrm{c} = s\tan\beta$ and the free energy can be written:

$$\mathscr{U} = \gamma_\mathrm{lv}\left[9\pi V^2(2+\cos\alpha)(1-\cos\alpha)^2\right]^{1/3} + \frac{3V\gamma_\mathrm{lv}}{\tan\beta}\frac{\cos^4(\alpha/2)}{2+\cos\alpha}s^{-1}. \tag{8}$$

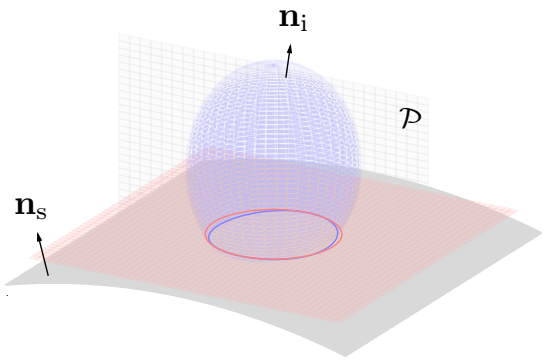

(a)

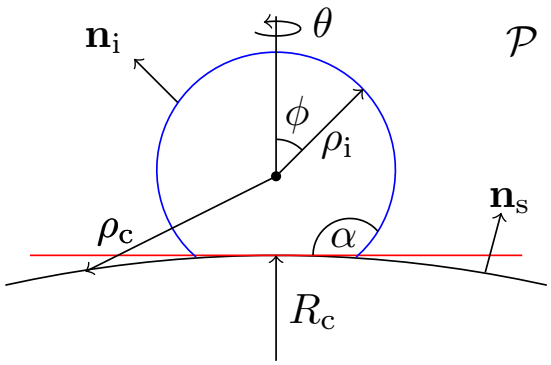

(b)

Fig. 4 A perturbed droplet in equilibrium on a cylindrical surface (gray) with the original unperturbed tangent plane shown in red. The red curve depicts the circular contact line of the droplet on a flat substrate while the blue curve depicts the perturbed contact line when the droplet is on a cylindrical substrate. The plane $\mathscr{P}$ cuts the schematic; the cross-section in (b) is shown with the variables and parameters employed in our theoretical formulation.

By taking the gradient of the energy, we find the force due to the curvature gradient to be

$$F_\mathrm{curv} = -\frac{\mathrm{d}\mathscr{U}}{\mathrm{d}s} = \frac{3\gamma V}{\cot\beta}\frac{\cos^4(\alpha/2)}{2+\cos\alpha}s^{-2}, \tag{9}$$

as presented in Galatola [19]. With this expression, a scaling argument suggests that the assumption that the effect of the cylindrical curvature dominates compared to the change in the radius of curvature over the droplet scale is valid provided that $\varepsilon\tan\beta \ll 1$, which in turn is consistent with our assumption that $\varepsilon \ll 1$.

We note that the force in (9) does not change sign as the contact angle α varies in the interval $[0,\pi]$: the curvature force always acts to push the drop towards the base of the cone (increasing s), independent of wettability, as has been observed experimentally. To gain some intuition about this surprising independence of wettability, we note that the contact line recedes radially on the perturbed substrate. This leads to an increase in the liquid–vapour area of $2\pi\varepsilon a_0\sin\alpha + 4\pi\varepsilon(1-\cos\alpha)\bar{\rho}_\mathrm{l}$ where $\bar{\rho}_\mathrm{l}$ is the average deformation of the interface and is found to be negative — that is, the contact line moving inwards causes the drop interface to, on average, be pulled inwards. The liquid–solid area also has two contributions: $2\pi\varepsilon a_0\tan\alpha$ and $-(\varepsilon\pi/2)(\sin^4\alpha/\cos\alpha)$. The first term comes from the contact line moving and covering more area while the second term is due to the substrate curvature. Once energy is considered and the liquid–substrate area is multiplied by a factor of $\cos\alpha$ the contact line contributions cancel out and the free energy perturbation comes from the lost liquid–vapour energy $4\pi\varepsilon(1-\cos\alpha)\bar{\rho}_\mathrm{l}$ and gained liquid–solid energy $\varepsilon\pi\sin^4\alpha/2$ resulting in $\delta\mathscr{U} = \pi\sin^4\alpha/4$. Since this function of α is always positive, the sign of the resulting force is independent of whether the droplet is wetting or non-wetting. Finally, we note that a droplet on the inside of a cone corresponds to $\varepsilon < 0$, and hence the force changes its sign: droplets inside cones move to the apex as reported previously.[13]

3.2 Viscous resistance

The force driving droplet motion is balanced by the friction due to the viscous dissipation in both the droplet and the lubricating liquid. Work by Keiser *et al.*[30] on a droplet sliding down an inclined plane under gravity demonstrated that when the lubricating oil is considerably more viscous than the droplet then the primary source of dissipation is flow within the meniscus surrounding the drop (which may be seen in Fig. 2). Furthermore, Keiser *et al.*[30] showed experimentally that the friction force due to the oil 'skirt' surrounding the droplet scales as $F_\mathrm{o} \sim \gamma_\mathrm{o} R(\lambda\eta_\mathrm{o}U/\gamma_\mathrm{o})^{2/3}$, where λ is a constant arising from truncating an integral at physically relevant scales.[35] Similar results have been found by Daniel *et al.*[31]. Using the data from Keiser *et al.*[30], we can determine the prefactor in their scaling to be approximately 9 and write,

$$F_\mathrm{o} = 9f\gamma_\mathrm{o}R_0\,(\lambda\mathrm{Ca}_\mathrm{o})^{2/3}, \tag{10}$$

where f denotes the covering fraction of the microstructure, $R_0 = R_\mathrm{d}\sin\alpha$ is the radius of the drop's footprint on a flat substrate and $\mathrm{Ca}_\mathrm{o} = \eta_\mathrm{o}U/\gamma_\mathrm{o}$ is the capillary number of the droplet's motion.

The driving force due to the gradient in curvature will be balanced by the viscous dissipation in (10) to find an equation for s, the displacement of the drop along the cone. Balancing Equations (9) and (10), and noting that $\mathrm{Ca}_\mathrm{o} = \eta_\mathrm{o}\dot{s}/\gamma_\mathrm{o}$ we find that

$$4s^3\dot{s} = \sigma^4 \tag{11}$$

where

$$\sigma = \left(\frac{4V\gamma_\mathrm{o}}{\lambda\pi\eta_\mathrm{o}}\right)^{1/4}\left(\frac{\gamma_\mathrm{eff}}{f\gamma_\mathrm{o}}F(\alpha)\cot\beta\right)^{3/8} \tag{12}$$

and

$$F(\alpha) = \frac{\cos^4(\alpha/2)}{2(2+\cos\alpha)}\frac{\left(3(2+\cos\alpha)(1-\cos\alpha)^2\right)^{1/3}}{\sin\alpha}. \tag{13}$$

Integrating (11) we find that

$$s^4 = s_0^4 + \sigma^4 t, \tag{14}$$

where s_0 is the initial position of the droplet centre.

Equation (14) shows that $s \sim \sigma t^{1/4}$ for sufficiently late times,

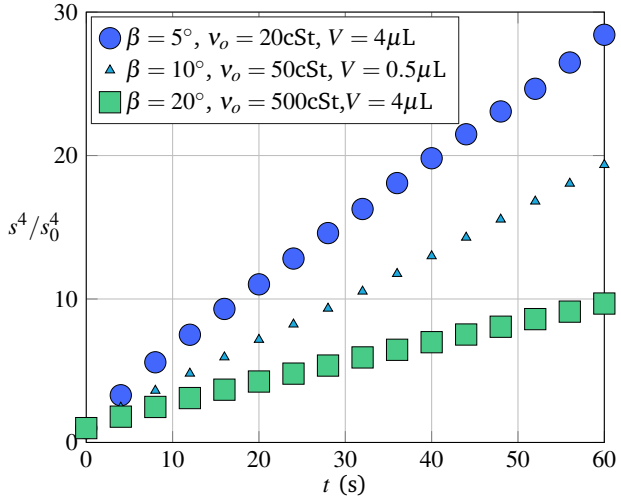

Fig. 5 Data from Fig. 2 replotted to show s^4 as a function of time, t. The linear relationship observed is in agreement with the prediction of Equation (14). Again, volumes are denoted by marker size and viscosities by marker colour as described by the legend.

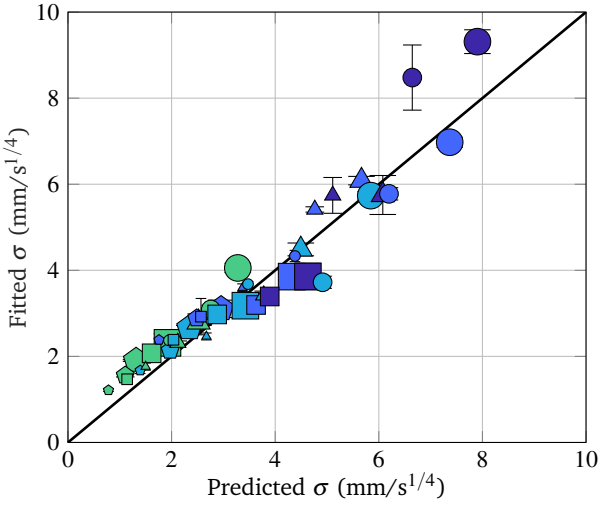

Fig. 6 Plot of the fitted values of the the coefficient in Equation (14) against the value predicted by Equation (12). Here, darker colours denote lower viscosity lubricating oils (20,50,500 cSt silicone oils and 12 cSt decanol), while the sizes of the markers denotes the volume of the droplet; finally, the shape denotes the cone half-angle β (●: $\beta = 5°$,▲: $\beta = 10°$, ■: $\beta = 20°$, ⬟: $\beta = 45°$).

explaining the scaling observed in the experimental results plotted in Fig. 3. More precisely, we require $t \gg (s_0/\sigma)^4$ to be in this 'late time' regime. Moreover, Fig. 5 confirms the prediction that s^4 is linear in time at earlier times too, with a constant offset because the droplet is not initially at the apex of the cone. From the experimental data, we compute a line of best fit of s^4 as a function of t. The fitted slope is found for each experiment and is plotted against the coefficient predicted by Equation (12) in Fig. 6. In plotting the prediction in Fig. 6, values of the dimensionless parameters f and λ are required. These parameters relate to the microstructure of the surface and a discussion of the appropriate values is included in Appendix A.

4 Non-conical axisymmetric substrates

Equation (7) for the free energy of the droplet can be readily generalized to non-conical substrates. Assuming that the surface is rotationally symmetric about its axis with local radius of curvature $R_c(s)$, and that variations in the radius are slow, we expect our cylindrical approximation to be appropriate and so,

$$\mathscr{U} \sim \text{const} + \gamma_{\text{eff}} V R_c(s)^{-1}. \tag{15}$$

Thus the force due to the curvature gradient is,

$$F_{\text{curv}} \sim \gamma_{\text{eff}} V \frac{R_c'(s)}{R_c^2}. \tag{16}$$

When balanced with the viscous forces arising from the lubricating oil layer (as discussed in Section 3.2) we find,

$$\frac{\mathrm{d}s}{\mathrm{d}t} \sim \left(\frac{\gamma_o}{\eta_o}\right) V \frac{R_c'(s)^{3/2}}{R_c^3}. \tag{17}$$

For simplicity, we consider the substrate's profile to be a power law, $y = x^n$ for $0 < n < 1$. Such a shape's radius of curvature is,

$$R_c(x) = y(x)\sqrt{1+y'(x)^2} = x^n\sqrt{1+n^2x^{2n-2}}, \tag{18}$$

where we have neglected the curvature in the direction of motion consistent with our slow variation assumption. The x-coordinate and arclength s are coupled through a differential equation,

$$\frac{\mathrm{d}s}{\mathrm{d}x} = \sqrt{1+n^2x^{2n-2}}. \tag{19}$$

This coupling means we may only solve for s numerically. However, we expect large displacements and small slopes at late times so that $s \sim x$ and,

$$\frac{\mathrm{d}x}{\mathrm{d}t} \sim \frac{1}{x^{3n}\sqrt{1+n^2x^{2n-2}}}\left(\frac{n(x^2+n(2n-1)x^{2n})}{(x^{3-n}+n^2x^{1+n})(1+n^2x^{2n-2})}\right)^{3/2}, \tag{20}$$

$$\sim \left(\frac{n}{x^{n+1}}\right)^{3/2}. \tag{21}$$

Thus, at late times,

$$x \sim n^{3/(5+3n)} t^{\frac{2}{5+3n}}. \tag{22}$$

Interestingly, the expression (22) shows that the late-time exponent, $2/(5+3n)$, is largest for the smallest shape exponents n; however, as $n \to 0$, the prefactor in the scaling vanishes too: droplets do not move on cylindrical substrates since the driving force vanishes. This is because the force is more sensitive to the curvature of the substrate than the substrate gradient. Note, however, that this scaling assumes that the viscous dissipation is dominated by that within the lubricating layer; if, for example, viscous dissipation were to occur predominantly *within* the droplet, other scalings may be exhibited.

5 Conclusion

We have presented a series of systematic experiments for droplets on lubricant infused cones and studied the dynamics of the droplet migration, or curvotaxis. By balancing the forces acting on the droplet, we showed that for sufficiently late times,

$s \sim \sigma t^{1/4}$. We also calculated the pre-factor σ and showed good agreement with our experimental results. We have used a dissipation law tested in detail in Keiser *et al.*[30] and whose precise domain of validity remains to be fully explored. However, since some features of the lubricating film (e.g. its thickness) enter at most logarithmically[30,31], we expect that the results derived should hold well beyond those confirmed explicitly here. We note that our results, in which contact line friction dominates inertia, suggest that droplets slow down as they move and, further, that the distance travelled within a given interval of time decreases with decreasing droplet size. However, such behaviour is friction-law dependent and hence differs from the results of Lv *et al.*[13].

Lastly, we briefly discussed how our theory can be extended to consider the case of non-conical substrates. Curvotaxis has already been shown to be useful in designing new technologies in fog harvesting for example[3]. However, if droplet motion via curvature gradients is to be achieved, then lubricant infused surfaces are indeed quite promising. Such surfaces can be manufactured straightforwardly which is essential for adoption in industry. More valuable again, is the *ease* with which wettability and therefore droplet morphology can be controlled. Reducing the effect of spreading allows for more predictable and controllable droplet motion. We also hope that our discussion of the dynamics of curvotaxis in the generalized setting of Section 4 might lead to analyses of drop motion in non-axisymmetric geometries; one possibility would be to investigate whether droplets move spontaneously on the cone-like aggregates of fibres that form when droplets wet a series of fibres[36].

Conflicts of interest

There are no conflicts to declare.

Acknowledgements

This work was financially supported by the Royal Society (URF\R\180016, and RGF\EA\181002), and through an Equipment Award from the Department of Engineering Science, Oxford.

References

1 P. Yager, T. Edwards, E. Fu, K. Helton, K. Nelson, M. R. Tam and B. H. Weigl, *Nature*, 2006, **442**, 412–418.

2 H. Andrews, E. Eccles, W. Schofield and J. Badyal, *Langmuir*, 2011, **27**, 3798–3802.

3 D. Chen, J. Li, J. Zhao, J. Guo, S. Zhang, T. A. Sherazi, Ambreen and S. Li, *J. Colloid Interf. Sci.*, 2018, **530**, 274–281.

4 N. Miljkovic, R. Enright, Y. Nam, K. Lopez, N. Dou, J. Sack and E. N. Wang, *Nano Lett.*, 2013, **13**, 179–187.

5 F. Brochard, *Langmuir*, 1989, **5**, 432–438.

6 N. Bjelobrk, H. L. Girard, S. B. Subramanyam, H. M. Kwon, D. Quéré and K. K. Varanasi, *Phys. Rev. Fluids*, 2016, **1**, 063902.

7 M. Prakash, D. Quéré and J. W. Bush, *Science*, 2008, **320**, 931–934.

8 P. Renvoisé, J. Bush, M. Prakash and D. Quéré, *EPL (Europhysics Letters)*, 2009, **86**, 64003.

9 E. Reyssat, *J. Fluid Mech.*, 2014, **748**, 641–662.

10 A. Ghosh, R. Ganguly, T. M. Schutzius and C. M. Megaridis, *Lab Chip*, 2014, **14**, 1538–1550.

11 É. Lorenceau and D. Quéré, *J. Fluid Mech.*, 2004, **510**, 29–45.

12 J.-L. Liu, R. Xe, B.-W. Li and X.-Q. Feng, *Chinese Phys. Lett.*, 2007, **24**, 3210–3213.

13 C. Lv, C. Chen, Y. C. Chuang, F. G. Tseng, Y. Yin, F. Grey and Q. Zheng, *Phys. Rev. Lett.*, 2014, **113**, 026101.

14 Y. Zheng, H. Bai, Z. Huang, X. Tian, F. Q. Nie, Y. Zhao, J. Zhai and L. Jiang, *Nature*, 2010, **463**, 640–643.

15 J. Ju, H. Bai, Y. Zheng, T. Zhao, R. Fang and L. Jiang, *Nat. Comm.*, 2012, **3**, 1247.

16 Q. Wang, X. Yao, H. Liu, D. Quéré and L. Jiang, *Proc. Natl. Acad. Sci.*, 2015, **112**, 9247–9252.

17 K. Li, J. Ju, Z. Xue, J. Ma, L. Feng, S. Gao and L. Jiang, *Nat. Comm.*, 2013, **4**, 2276.

18 T. Mouterde, G. Lehoucq, S. Xavier, A. Checco, C. T. Black, A. Rahman, T. Midavaine, C. Clanet and D. Quéré, *Nat. Mater.*, 2017, **16**, 658–663.

19 P. Galatola, *Phys. Rev. Fluids*, 2018, **3**, 103601.

20 T. S. Chan, F. Yang and A. Carlson, *arXiv preprint arXiv:1901.03548*, 2019.

21 G. McHale, M. I. Newton and B. J. Carroll, *Oil Gas Sci. Tech.*, 2001, **56**, 47–54.

22 H. B. Eral, J. De Ruiter, R. De Ruiter, J. M. Oh, C. Semprebon, M. Brinkmann and F. Mugele, *Soft Matter*, 2011, **7**, 5138–5143.

23 T. H. Chou, S. J. Hong, Y. E. Liang, H. K. Tsao and Y. J. Sheng, *Langmuir*, 2011, **27**, 3685–3692.

24 Y. Li, H. Wu and F. Wang, *J. Phys. D: Appl. Phys.*, 2016, **49**, 085304.

25 M. Shanahan, *Langmuir*, 2011, **27**, 14919–14922.

26 J. Ju, K. Xiao, X. Yao, H. Bai and L. Jiang, *Adv. Mater.*, 2013, **25**, 5937–5942.

27 H. Bai, X. Tian, Y. Zheng, J. Ju, Y. Zhao and L. Jiang, *Adv. Mater.*, 2010, **22**, 5521–5525.

28 Y. E. Liang, H. K. Tsao and Y. J. Sheng, *Langmuir*, 2015, **31**, 1704–1710.

29 T.-S. Wong, S. H. Kang, S. K. Tang, E. J. Smythe, B. D. Hatton, A. Grinthal and J. Aizenberg, *Nature*, 2011, **477**, 443–447.

30 A. Keiser, L. Keiser, C. Clanet and D. Quéré, *Soft Matter*, 2017, **13**, 3404–3410.

31 D. Daniel, J. V. Timonen, R. Li, S. J. Velling and J. Aizenberg, *Nat. Phys.*, 2017, **13**, 1020–1025.

32 J. H. Guan, É. Ruiz-Gutiérrez, B. B. Xu, D. Wood, G. McHale, R. Ledesma-Aguilar and G. G. Wells, *Soft Matter*, 2017, **13**, 3404–3410.

33 F. Schellenberger, J. Xie, N. Encinas, A. Hardy, M. Klapper, P. Papadopoulos, H. J. Butt and D. Vollmer, *Soft Matter*, 2015, **11**, 7617–7626.

34 C. Urata, B. Masheder, D. F. Cheng and A. Hozumi, *Langmuir*, 2013, **29**, 12472–12482.

35 P.-G. De Gennes, F. Brochard-Wyart and D. Quéré, *Capillar-*

ity and Wetting Phenomena: Drops, Bubbles, Pearls, Waves, Springer, 2013.

36 C. Duprat, S. Protière, A. Y. Beebe and H. A. Stone, *Nature*, 2012, **482**, 510–513.

Appendix A: Experimental details

Manufacture of SLIPS

Brass cones were machined using a lathe and then progressively polished to 12000 grit (Micro-mesh abrasives). Three coats of Glaco were then applied in 30 minute intervals. Lastly, silicone oil (Sigma-Aldrich) was applied with a syringe and the excess was removed using compressed air.

Comparing experiment and theory

In going from Equation (10) to Equations (14) and (12) we have replaced the unperturbed contact line radius R_0 with the volume which are related by $R_0^3 = 3V\sin^3\alpha/(\pi(2+\cos\alpha)(1-\cos\alpha)^2)$. We also note that the surface tension in the driving force has been replaced by γ_{eff} which may have two values: $\gamma_{\text{eff}} = \gamma_{\text{ow}} + \gamma_{\text{oa}}$ (if a layer of oil cloaks the droplet) or $\gamma_{\text{eff}} = \gamma_{\text{wa}}$ (if not). Silicone oil has been shown to coat the surface of a water drop however, this does not occur in the case of decanol[33].

When comparing the predicted and theoretical values of σ, we let $f = 1$ and $\lambda = 10$. These parameters depend on the Glaco microstructure. However, since the Silica beads are ~ 30 nm we assume there is a uniform coating and let $f = 1$. The value of $\lambda = \ln(\ell/a)$ where ℓ is a scale for the size of the viscous wedge and a is represents molecular scales.[35] For Glaco, the value of λ has been reported to be $\lambda \sim 10$.[30]

Appendix B: Details of asymptotic approach

Expanded Young–Laplace equation

The Young–Laplace equation in spherical coordinates is,

$$p/\gamma = \frac{2}{S\rho_{\text{i}}} - \frac{1}{\rho_{\text{i}}\sin\phi}\left\{\frac{\partial}{\partial\phi}\left[\frac{\sin\phi}{\rho_{\text{i}}S}\frac{\partial\rho_{\text{i}}}{\partial\phi}\right] + \frac{\partial}{\partial\theta}\left[\frac{1}{\rho_{\text{i}}S\sin\phi}\frac{\partial\rho_{\text{i}}}{\partial\theta}\right]\right\}, \tag{B.1}$$

where,

$$S = \left[1 + \left(\frac{1}{\rho_{\text{i}}}\frac{\partial\rho_{\text{i}}}{\partial\phi}\right)^2 + \left(\frac{1}{\rho_{\text{i}}\sin\phi}\frac{\partial\rho_{\text{i}}}{\partial\theta}\right)^2\right]^{1/2}. \tag{B.2}$$

We assume that $\rho_{\text{i}} = R_d + \varepsilon\rho_{\text{i},1}(\phi,\theta) + O(\varepsilon^2)$ and $p = p_0 + \varepsilon p_1 + O(\varepsilon^2)$. The Young–Laplace equation then reads, to $O(\varepsilon^2)$,

$$\frac{p_0+\varepsilon p_1}{\gamma} = \frac{2}{R_{\text{d}}} - \frac{\varepsilon}{R_{\text{d}}^2}\left(2\rho_{\text{i},1} + \rho_{\text{i},1,\theta\theta}\csc^2\phi + \rho_{\text{i},1,\phi}\cot\phi + \rho_{\text{i},1,\phi\phi}\right). \tag{B.3}$$

Cylinder in Spherical Coordinates

A cylindrical substrate, parallel to the y-axis, has

$$x^2 + [z_{\text{sub}} - (R_{\text{d}}\cos\alpha - R_{\text{c}})]^2 = R_{\text{c}}^2. \tag{B.4}$$

We non-dimensionalize lengths with the radius of curvature of the droplet on a flat substrate, R_{d}, and pressure with γ/R_{d}. In particular, we let $\hat\rho_{\text{i}} = \rho_{\text{i}}/R_{\text{d}}$, $\hat\rho_{\text{c}} = \rho_{\text{c}}/R_{\text{d}}$ and $\hat p = pR_{\text{d}}/\gamma$ and similarly with their expansion in powers of ε. Then, written in spherical coordinates, and expanded to $O(\varepsilon^2)$,(B.4) becomes

$$\varepsilon\hat\rho_{\text{c}}\cos\phi = -1 + \varepsilon\cos\alpha + \left(1 - \varepsilon^2\hat\rho_{\text{c}}^2\sin^2\phi\cos^2\theta\right)^{1/2}, \tag{B.5}$$

and hence

$$\hat\rho_{\text{c}}\cos\phi \sim \cos\alpha - \varepsilon\frac{\hat\rho_{\text{c}}{}^2\sin^2\phi\cos^2\theta}{2}. \tag{B.6}$$

Equation (B.6) is a quadratic for $\hat\rho_{\text{c}}$ which can be solved to find,

$$\hat\rho_{\text{c}} = \frac{\cos\alpha}{\cos\phi} - \varepsilon\left(\frac{\cos^2\alpha\sin^2\phi\cos^2\theta}{2\cos^3\phi}\right). \tag{B.7}$$

Boundary Conditions

The contact line is parameterized as $\hat\rho = \hat\rho_{\text{c}}$, $\phi = \alpha + \varepsilon f(\theta)$. It can be shown that due to the symmetry of the substrate, $f(\theta) = a_0 + a_1\cos(2\theta)$. With this, the boundary conditions become,

$$\hat\rho_{\text{i},1}(\alpha,\theta) = \left(a_0 - \frac{\sin\alpha}{4}\right)\tan\alpha + \left(a_1 - \frac{\sin\alpha}{4}\right)\tan\alpha\cos(2\theta), \tag{B.8}$$

$$\left.\frac{\partial\hat\rho_{\text{c},1}}{\partial\phi}\right|_{\phi=\alpha} = a_0 - \frac{\sin\alpha}{2} + \cos(2\theta)\left(a_1 - \frac{\sin\alpha}{2}\right). \tag{B.9}$$

The $O(\varepsilon)$ problem

We make the substitution, $\hat\rho_{\text{c},1}(\phi,\theta) = U(\phi,\theta) - \hat p_1/2$, which makes Equation (B.3) homogeneous. The problem at $O(\varepsilon)$ is then,

$$\nabla^2 U + 2U = 0, \tag{B.10}$$

$$U(\alpha,\theta) = \frac{\hat p_1}{2} + a_0\tan\alpha - \frac{\sin\alpha\tan\alpha}{4} + \cos(2\theta)\left(a_1\tan\alpha - \frac{\sin\alpha\tan\alpha}{4}\right), \tag{B.11}$$

$$\left.\frac{\partial U}{\partial\phi}\right|_{\phi=\alpha} = a_0 - \frac{\sin\alpha}{2} + \cos(2\theta)\left(a_1 - \frac{\sin\alpha}{2}\right). \tag{B.12}$$

Equation (B.10) can be solved via separation of variables to find,

$$U = C_1\cos\phi + (C_2\cos2\theta + C_3\sin2\theta)\left(\frac{\cos\phi - (1/3)\cos^3\phi}{\sin^2\phi} - \frac{2}{3}\frac{1}{\sin^2\phi}\right). \tag{B.13}$$

Imposing the boundary conditions we find that $C_3 = 0$ and,

$$C_1 = \frac{1}{4}\left(2\hat p_1\cos\alpha + \sin^2\alpha\right), \tag{B.14}$$

$$C_2 = \cos^4(\alpha/2), \tag{B.15}$$

$$a_0 = \frac{\sin\alpha}{8}\left[3 - 4\hat p_1\cos\alpha + \cos(2\alpha)\right], \tag{B.16}$$

$$a_1 = \cos\left(\frac{\alpha}{2}\right)\sin^3\left(\frac{\alpha}{2}\right)\frac{3+\cos\alpha}{3}. \tag{B.17}$$

To solve for the pressure perturbation, we impose conservation

of volume,

$$\frac{V}{R_{\mathrm{d}}^3} = \int_0^{2\pi} \int_0^{\alpha+\varepsilon f(\theta)} \int_0^{1+\varepsilon u} dV + \int_0^{2\pi} \int_{\alpha+\varepsilon f(\theta)}^{\pi} \int_0^{\hat{\rho}_{\mathrm{c},0}+\varepsilon\hat{\rho}_{\mathrm{c},1}} dV. \tag{B.18}$$

(Note that the left-hand-side of (B.18) is a function of the contact angle α.) Performing the integration and setting equal to zero the $O(\varepsilon)$ perturbation we find that,

$$\hat{p}_1 = \frac{3\cos^4(\alpha/2)}{2+\cos\alpha}. \tag{B.19}$$